J. Geophys. 42, 633–644, 1977

Journal of Geophysics

A Survey on Measurements of Medium Energy Protons and Electrons Obtained with the Particle Spectrometer E8 on Board of Helios

E. Keppler*, A.K. Richter, K. Richter, G. Umlauft, B. Wilken, and D.J. Williams**

Max-Planck-Institut für Aeronomie, D-3411 Katlenburg-Lindau 3, Federal Republic of Germany

Abstract. We briefly describe a magnetic particle spectrometer for measuring protons ($E > 80$ keV) and electrons ($E > 15$ keV), flown on Helios-1 and -2. Showing examples of measurements obtained in interplanetary space, we show the capability of the instrument to resolve structures in time with 13 s resolution, and demonstrate the importance of having this high time resolution. A second feature is its energy resolution, which for the first time allows for precise measurements in this energy domain. A third feature is the angular resolution in 16 sectors. Again we demonstrate, that having this resolution is indispensable for correct interpretation of data. By combining these features, we are able to apply the Compton-Getting transformation without a priori assumptions.

Key words: Helios spacecrafts – Solar wind protons – Solar wind electrons.

1. Introduction

Helios-1 (launched Dec. 10, 1974) and Helios-2 (launched Jan. 15, 1976) are in orbits around the sun with aphels of ~1 AU, and perihels of 0.31 and 0.29 AU, respectively. While Helios-1's antenna is pointing northward, Helios-2 operates upside down. Both spacecraft are spinning in the same sense at a rate of about 1 rotation per second, with the spin axis normal to the ecliptic plane, Helios-1 counter-clock-wise, when viewed from the north.

Both spacecraft are operating almost perfectly since launch, and have been tracked by the DSN-ground-network and by the German stations Effelsberg and Weilheim. This allowed for very good data coverage since launch. In addition, when the spacecraft are not viewed by antennas, they are put into a storage mode, where, dependent upon the time gap to the next receiving period, the data

* To whom offprint requests should be sent

** Permanent address: NOAA-ERL-SEL, Boulder, CO, USA

are stored in the 500 kbit memory of the S/C, utilizing low bitrate and eventually a certain data frame deletion rate. Due to this peculiarity, Helios data are obtained for 24 h/day, even if there is realtime coverage only for a fraction per day. For this reason, Helios became the spacecraft with the most complete data coverage since launch. As all instruments are working nominally and also the S/C is in good condition, it is hoped to have this continued for quite a while.

2. The Charged Particle Spectrometer E8

The instrument uses an inhomogeneous magnetic field to separate electrons and ions and detect them by using separate semiconductor surface barrier detectors. The instrument utilizes a geometrical factor, which is $1.5 \cdot 10^{-2}$ cm^{2}ster for ions, and $\leqq 5 \cdot 10^{-2}$ cm^{2}ster for electrons. Due to the operational principle (Fig. 1), electrons are deflected according to their rigidity; thus each of the detectors covers a certain energy range. The design of the magnetic system realizes focussing of electrons in a certain energy range. As this feature disappears with increasing energy, efficiency degrades somewhat. As a result of this, efficiency is a function of energy as shown in Figure 2. Efficiency has been measured in an electron spectrometer. Curves in Figure 2 are least square fits to the measurements. Efficiency is in this context being defined by the ratio of the actual count rate of a particular detector at a given energy to the counting rate of a reference detector of sensitive area equal to the entrance aperture, moved to replace the aperture before and after the measurement. So efficiency, as defined here, does not take into account backscattering. However, this effect tends to be cancelled out by the applied technique, so we feel that our figures are uncertain by a few % only.

The signals from each detector are amplified and fed to a 16-channel-pulseheight-analyzer. The energy range covered is 20 keV to 2 MeV. Channel allocation is given in Table 1.

Protons and ions are almost unaffected by the magnetic field (800 Gauss maximum) and are detected in a telescope arrangement. Again the front detector signal is analyzed in 16 channels (see Table 1) in anticoincidence with the backdetector signal. The frontdetector is covered by a 120 μg/cm^2 Al-layer. Correspondingly, protons are analyzed above 80 keV (utilizing $\Delta E \geqq 20$ keV of energy loss in the frontdetector). Alpha particles contribute to the various energy channels if their energy is $E \gtrsim 100$ keV. Particle entrance is through the aluminium layer. All detectors are surface barrier detectors, fully depleted, operated at about 150 % overbias.

The energy ranges for the various channels are shown in Table 1. All channels, except where indicated, are differential of the form $\overline{D_i D_{i+1}}$. Channel width is quasilogarithmically increasing. In addition to the differential channels, integral channels are formed. The latter are used to obtain simultaneously the intensity from 16 directions, ions and electrons being obtained in alternating sequence.

The instrument is mounted on the spacecraft to include an angle of 7° with the normal to the spin axis, thus scanning approximately within the ecliptic

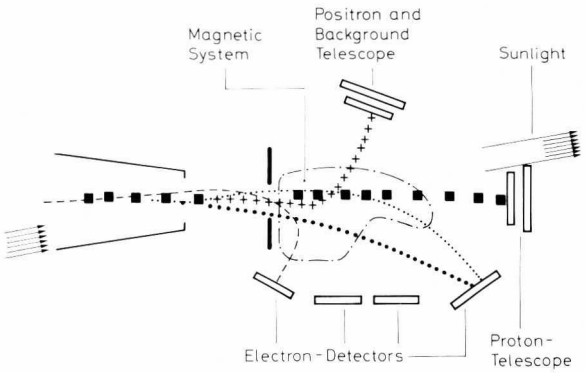

Fig. 1. Particle separation in the magnetic spectrometer E8, schematically. An inhomogeneous magnetic field is applied to improve efficiency by focussing

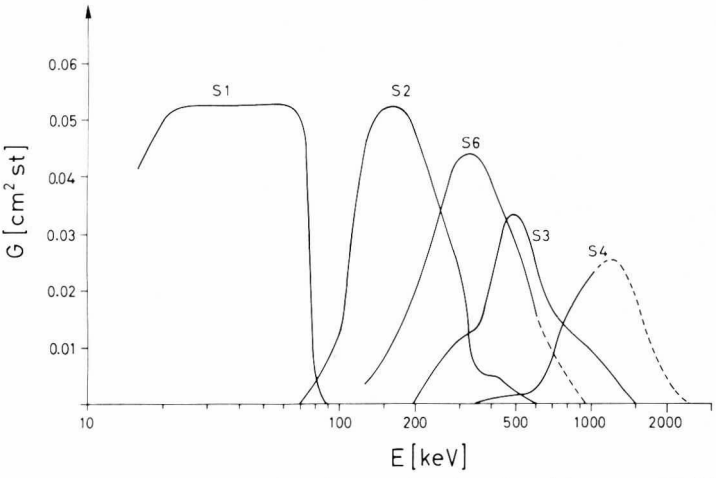

Fig. 2. Efficiency of electron detection as a function of particle energy. S1–S4 are electron detectors, covering different energy ranges: S1: 16–100 keV; S2: 90–350 keV; S3: 230–850 keV; S4: 600–2000 keV

plane (opening angle 20° full angle). While spinning, data collection is being sectorized in 16 sectors. A set of integral rates from all 16 sectors is obtained alternating between ions and electrons. Energy spectra from ions and electrons are obtained from all 16 directions subsequently, two at a time. The time resolution, which will be obtained, is bitrate dependent; the Helios bitrate may be varied from 8–4096 bps. The instrument is adjusted to bitrate changes by changing the accumulation time (maintaining the sectorization) correspondingly. At the highest bitrate the highest time resolution, which may be achieved for angular distributions, is 13.5 s, while a full set of energy spectra from 16 directions takes 108 s. At low bitrate a reduced format is used, which, at 8 bps, provides a full set of information from 8 sectors (instead of 16) in 19 min.

Table 1. Energy channels for protons and electrons (in keV)

	Channel No.															Integral	Coincidence
	1	2	3	4	5	6	7	8	9	10	11	12	13	14	15	16		
Protons																		
Helios-1	80	87	96	105	117	130	146	165	190	225	267	320	390	475	585	730	$>20, >134$	>6200
Helios-2	87	95	102	110	121	135	153	176	200	235	280	340	415	500	620	750	$>21, >137$	>6200
Electrons																		
Helios-1	17	22	28	35	46	58	74	92	120	155	202	250	325	412	525–2000		16	
Helios-2	20	25	32	41	52	62	80	102	125	158	201	254	324	411	519–2000		19	

Table 2. Sectorization

	Sector number															
	1	2	3	4	5	6	7	8	9	10	11	12	13	14	15	16
Helios-1				Sun				East				Anti-sun				West
Helios-2				Sun				West				Anti-sun				East

Sector formation is done such, that the sector pattern remains fixed relative to the sun throughout the mission, sector 4 always facing the sun. Due to the opposite orientation of Helios-1 and -2, the direction of sectors relative to the S/C-sun-line ("west" being in the right side, when viewing towards the sun) is as given in Table 2.

3. Data Evaluation

While ion detection is performed through a two-element-telescope arrangement (coincidence signals are used to suppress analysis of frontdetector signals, coincidence resolution time is 0.8 μs), which provides for a reasonable background suppression, electron detectors are not protected by anticoincidence detectors, and therefore suffer from the 4π cosmic ray background. As this was anticipated, a backgrounddetector has been included into the instrument, which is completely protected from being reached by particles entering through the aperture. Both, electron detectors and backgrounddetector are shielded by the same amount of matter (2.5 g/cm^2, average) equivalent to 4 MeV electron range or 46 MeV for protons. The backgrounddetector is monitored by a 80 keV electronic threshold, well below the energy loss of minimum ionizing particles in a 300 μm detector, sufficient to provide for Landau spread. The counting rate of the backgrounddetector is being transmitted along with each data sample, thus allowing for determination of the penetrating particle flux.

For data presentation the following procedure is applied on a routine basis: During quiet times the ratio λ_i of the counting rate N_{iq} for each channel to the backgrounddetector counting rate N_{uq} is being determined throughout the mission. Thus for all data channels the true rate N_i^* is being calculated by $N_i^* = N_i - \lambda_i N_u$. Conversion to differential fluxes j_i is obtained by

$$j_i = \frac{N_i^*}{k_i G_i \Delta E_i} \tag{1}$$

where G_i is the effective geometric factor (0.015 cm^{2}ster for protons, for electrons as given by Figure 2 (S1, S2, S3, S4)); ΔE_i is the differential energy interval $\Delta E_i = E_{i+1} - E_i$, summarized in Table 1; k_i is a filter correction factor, which is calculated from the actual channel noise figure σ kev (RMS) (determined during inflight calibration periods) by

$$k_i = \frac{\int_{U_i}^{U_{i+1}} j(E(U))\, dU}{\int_0^\infty j(E(U))\, F(U, \sigma)\, dU}. \tag{2}$$

In Equation (2) U is the energy deposited in the detector, E is the kinetic energy of the particle. $E(U)$ takes into account that a particle looses energy in the deadlayer of the detector; it is determined experimentally for protons, while for

electrons $E \approx U$. $F(z)$ is the filter function defined by the properties of the pulseheight-analyzer

$$F(z) = \tfrac{1}{2}(\operatorname{erf} z - \operatorname{erf}(z - a_i)) \tag{3}$$

$\left(z = \dfrac{U - U_i}{\sqrt{2}\sigma};\ a_i \dfrac{\Delta E_i}{\sqrt{2}\sigma}\right)$. k_i therefore is the ratio of the channel rate which would be obtained for a noisefree channel, to the rate obtained in the real channel. For $j(E)$ a powerlaw $j(E) \sim E^{-\gamma}$ was adopted. The dependence of k_i on γ is very small for $\gamma \lesssim 5$, but rises beyond. It approaches unity when $\Delta U_i > 5\sigma$, as is to be expected (which is above channel 7 for protons, for electrons above channel 8).

This procedure of course is a first approximation, but of sufficient reliability for overview purposes. Whenever a detailed analysis is required, the energy spectrum will be calculated by solving the integral equation, which relates counting rate and differential flux. A similar procedure is being followed when angular distributions are evaluated, which significantly differ from isotropy, as has been shown by Richter (1972). Details are described by Keppler et al. (1976).

N_i^*, the true rate, is then, by definition zero (and of course may reach negative numbers for statistical reasons). The rates shown in Figure 9 are obtained through this procedure. This procedure is valid as long as background is due to galactic cosmic rays only (also during Forbush-type decreases), however breaks down if solar particles above some tens of MeV appear. Then to the CR-background rate a solar particle contribution is added which changes the ratio slightly. Then a more sophisticated procedure has to be applied. However, the difference is small as long as the energy spectrum is steep ($\gamma \geqq 4$), and is relevant only during low intensity electron events, where counting rates are close to background, as electron detectors suffer from the full 4π contribution. The proton detector is protected by the coincidence shield, therefore in this case these effects may be ignored.

The proton detector is also sensitive to heavier particles, however, is not able to resolve their contribution (along with protons, $E > 80$ keV, α-particles with $E \gtrsim 100$ keV will be measured). So for brevity we refer for the rest of the paper to protons, as probably most of the contributions to the detectors counting rate is due to protons.

4. Instrument Performance

In the following section we shall show a few examples of measurements, obtained during the mission in order to demonstrate the instrument's capability. We do not intend to discuss the physical meaning of the observations here in any depth. It is, however, our intention to show the significance of high resolution measurements in deep space.

Figure 3 shows as an example a 16-channel-energy-spectrum, obtained for ions, presumably protons, in the energy range 80–700 keV during the passage of Helios-1 through the dusk magnetosheath on December 10, 1974, averaged over time and direction. At the time of magnetosheath crossing, a magnetospheric

substorm was in progress ($K_p = 4^-$). It is likely, that these protons constitute a "proton burst", i.e. particles released from the tail region. Those events have been described in the literature quite often (e.g. Sarris et al., 1977). At the same time the APL-instrument on IMP-7 (Sarris, personal communication) being in interplanetary space on the sunward side of the magnetosphere has detected a burst with peak flux at 10 UT. We therefore tentatively assume that both instruments observed the same event.

In Figure 3 we also show the electron spectrum obtained during the electron burst at 10:20 UT (Fig. 4) at the time of magnetopause crossing, again averaged over all directions. While the proton spectrum is time averaged over 1 h, the electron spectrum is only averaged over 1 min. Consequently, the proton spectrum could be obtained through 4 orders of magnitude in intensity with good statistical significance, while the electron spectrum in higher energy channels becomes statistically insignificant.

Figure 4 shows the intensity variations of electron- and proton-integral rate channels along with the magnetic field data throughout the magnetosheath. Magnetopause and bowshock crossing have been tentatively marked. Full time resolution is being utilized (13 s). It is seen, that there are statistically significant intensity variations within time scales of minutes. These fluctuations resemble fluctuations of the magnetic field, in particular those of theta, the angle out of the ecliptic plane. The bowshock crossing is assumed to have occured at 10h 11 m 30s UT as indicated by the magnetic field variation, accordingly the proton flux decayed gradually at this time and reached background levels afterwards. Figure 5 shows two examples of angular distributions of protons during magnetosheath crossing. It is seen, that there are remarkable changes in the anisotropy. Clearly the anisotropy is much more pronounced when utilizing 16 sectors. It would have been considerably underestimated, if e.g. only 8 sectors would have been used. Data shown are raw data, i.e. background has not been subtracted, nor was the distribution transformed to the frame of reference comoving with the plasma (see below). This would have changed the proton angular distribution quite certainly.

In Figure 6 we demonstrate the third important feature of this instrument, which is the determination of the energy spectrum from 16 directions. Only proton spectra are shown, electron fluxes were too low. It is these spectra, from which Figure 3 has been constructed by averaging over all directions. Most remarkable is the deviation of the spectra from monotony at low energies in sectors 10–15 (anti-sun-direction). Plasma flow in the magnetosheath is generally in the anti-sun-direction. Therefore in transforming these spectra to the comoving plasma frame of reference, they tend to become "lifted" at the low energy end. It is to be expected therefore, that in most of the magnetosheath measurements after transformation (see Ipavich, 1974) to the plasma frame the spectra from all directions become the same, and the directional distribution, showing its maxima in the solar direction, becomes isotropic. We have not done this here as plasma data have not been available to us.

On the other hand we note, that the measurements indeed show different spectra in different directions as is to be expected. However, this example (Fig. 6) demonstrates, that it is incorrect to assume e.g. power law spectra and then

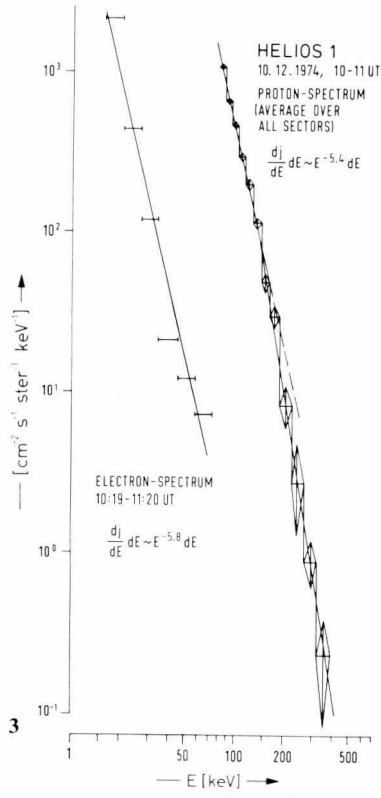
HELIOS 1
10. 12. 1974, 10-11 UT
PROTON-SPECTRUM
(AVERAGE OVER
ALL SECTORS)
$\frac{dj}{dE} dE \sim E^{-5.4} dE$
ELECTRON-SPECTRUM
10:19-11:20 UT
$\frac{dj}{dE} dE \sim E^{-5.8} dE$
10^3
10^2
10^1
10^0
10^{-1}
— [cm^{-2} s^{-1} ster^{-1} keV^{-1}] —
1
50
100
200
500
— E [keV] —

3

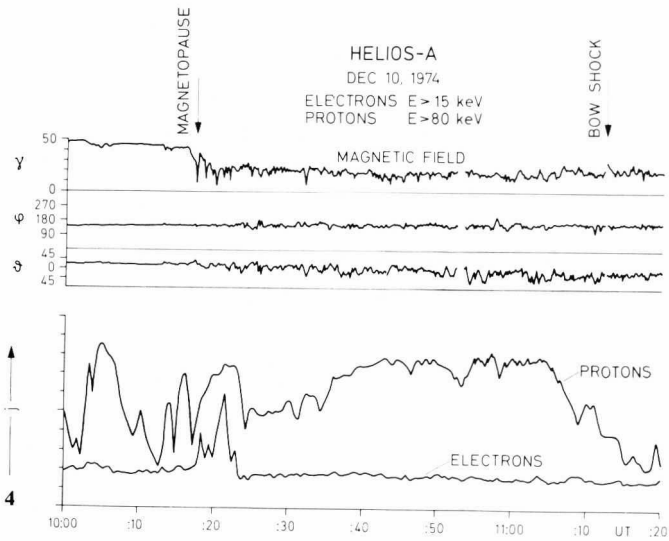
HELIOS-A
DEC 10, 1974
ELECTRONS E>15 keV
PROTONS E>80 keV
MAGNETOPAUSE
BOW SHOCK
MAGNETIC FIELD
γ
φ
ϑ
50
0
270
180
90
45
0
45
PROTONS
ELECTRONS
10:00
:10
:20
:30
:40
:50
11:00
:10
UT
:20

4

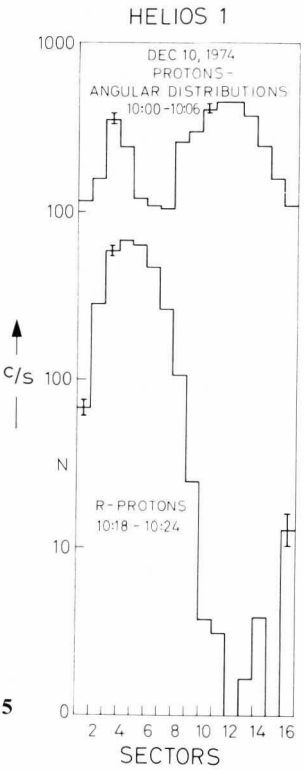
HELIOS 1
DEC 10, 1974
PROTONS -
ANGULAR DISTRIBUTIONS
10:00 - 10:06
R - PROTONS
10:18 - 10:24
1000
100
10
0
C/S
N
2 4 6 8 10 12 14 16
SECTORS

5

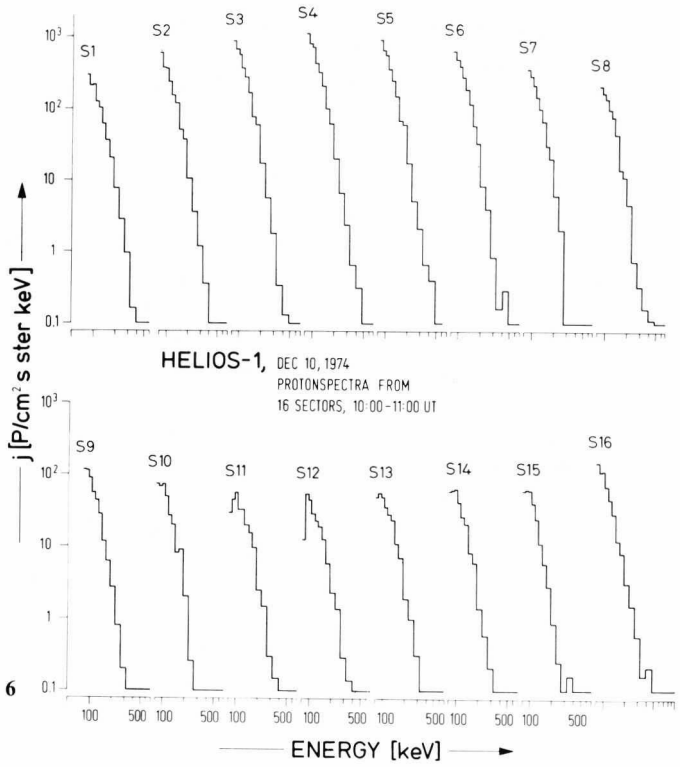
S1
S2
S3
S4
S5
S6
S7
S8
S9
S10
S11
S12
S13
S14
S15
S16
HELIOS-1, DEC 10, 1974
PROTONSPECTRA FROM
16 SECTORS, 10:00-11:00 UT
j [P/cm^2 s ster keV]
10^3
10^2
10
1
0.1
100
500
— ENERGY [keV] —

6

apply the Compton-Getting transformation. This has often been done in the past, because spectral informations were sometimes derived from counting rates in 2 or 3 energy ranges only. In applying the Compton-Getting transformation intensity, angle and energy are being transformed. However, the concept as outlined by Ipavich (1974), which starts from power law approximations in the spacecraft frame, is not generally applicable. This is also shown by Figure 8 (from Keppler et al., 1974), where for a proton event on January 6, 1975, power law fits ($E^{-\gamma}$) have been applied to the measured data. γ is seen to vary considerably in the spacecraft frame (observed), but do not result, after transformation, in a unique spectral slope. This would have been expected, as the angular distribution (similar to Fig. 7, middle of panel, right side) in this event fits nicely to a cosine in angle.

Having this in mind, the Compton-Getting transformation should not be biased by unrealistic assumptions on the energy spectrum in the S/C-frame, but rather start from the measured flux in given differential energy channels and directions. Applying this procedure (Richter et al., 1977), one obtains the correct transformation of flux, energy and angle to the comoving frame of reference without a priori assumption.

In Figure 7 several examples of measured angular distributions are shown. These measurements have been made after the spacecraft has been tilted with its spin axis now normal to the ecliptic plane (2 days after launch). Bidirectional and unidirectional distributions for protons are shown (right panel) together with a distribution obtained during quiet times. The left panel (Fig. 7) shows two examples of electron angular distributions. Close to perihel, one of the four electron detectors (S2, Fig. 1) suffers from straylight. Despite its $120\,\mu g/cm^2$ Al-contact, facing incoming particles, it was affected by light, if more than 6 solar constants where present. This was, however, restricted to the sun-viewing sector (No. 4) and did not affect the measurements as obvious from comparison of the two quiet time distributions (January 14, 1975 and March 5, 1975; perihel was on March 15, 1975).

In Figure 8 (left panel) we show as another example observations obtained during a proton event on March 18, 1975. Again (power law fits have been used here for simplicity) the spectral exponent is being determined in the 16 directions in the S/C frame. Using the solar wind velocity, this has been transformed to the solar wind frame to give the angular variation of the spectrum in the solar wind frame. It is seen, that in this case the differences in spectral slope are

Fig. 3. Proton and electron spectrum averaged in time and over all directions, for magnetosheath passage (December 10, 1974)

Fig. 4. Intensity variations of electrons ($E \geqq 16\,keV$) and protons ($E \geqq 80\,keV$) within the dusk magnetosheath shortly after Helios launch on December 10, 1974. Magnetic field data are shown along with the data (courtesy G. Musmann and F.M. Neubauer)

Fig. 5. Examples of angular distributions of electrons and protons (raw data) during magnetosheath crossing (December 10, 1974)

Fig. 6. Proton energy spectra from 16 different directions

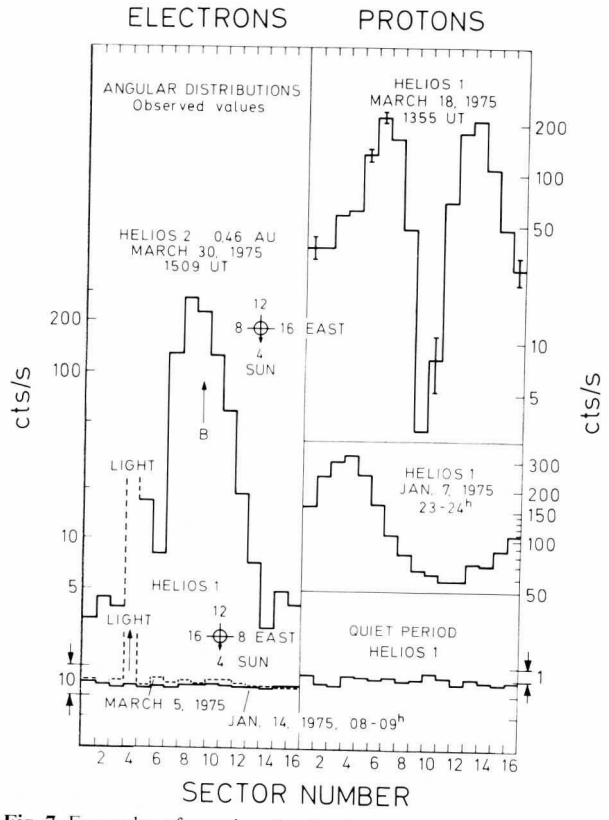

Fig. 7. Examples of angular distributions, measured with Helios-1 in interplanetary space (raw data)

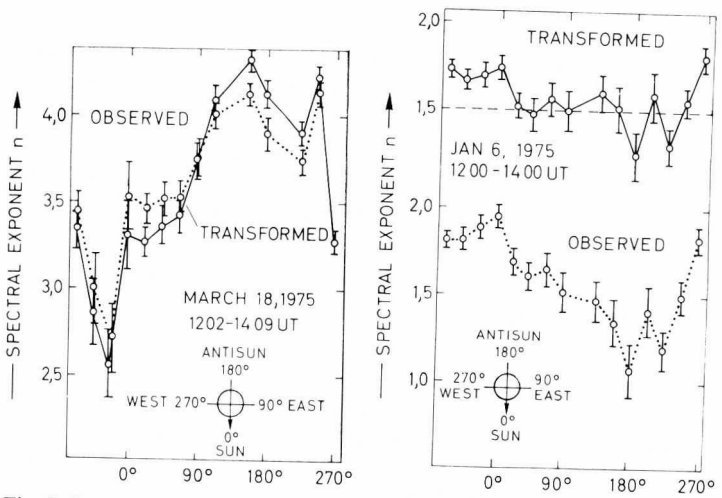

Fig. 8. Exponent of a power law fit to proton energy spectra from different directions, as observed and after being transformed to the frame of reference, comoving with the solar wind (Compton-Getting transformation)

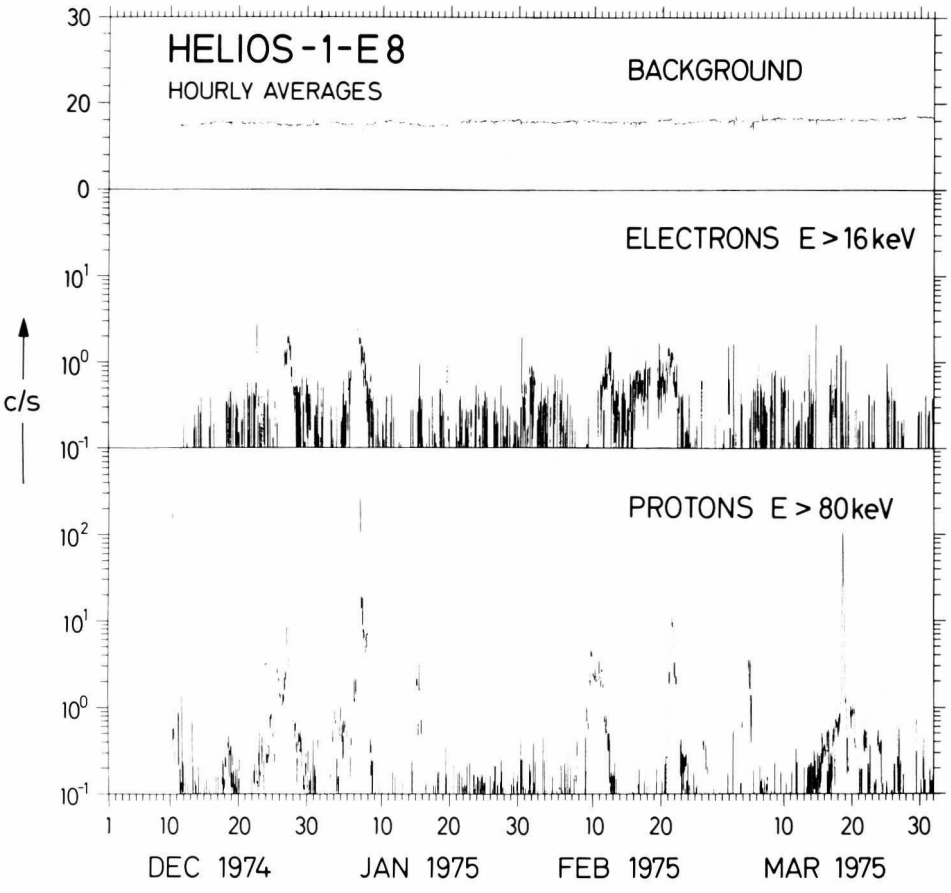

Fig. 9. Summary plot of 4 months of Helios-1 data, from launch to after perihelium. Proton- ($E \geqq 80$ keV) and electron- ($E \geqq 16$ keV) integral rates ae shown along with the backgrounddetector-rate. Background has been subtracted for both electron- and proton-rates

increased. This has to be interpreted as being indicative of different particle populations moving opposite to each other along the interplanetary field.

Figure 9 finally shows a summary of 4 months of Helios-1 data, displaying integral rates of protons (ions) ($E > 80$ keV), electrons ($E > 16$ keV) along with the backgrounddetector rate. Background has been subtracted by applying the procedure outlined in section 3. The scale has been cut off at 10^{-1} c/s, which is for this averaging time the limit below which no statistical meaningful conclusions may be drawn. Despite the fact that the sun was extraordinary quiet during this period, several events have been observed, some of which are corotating, some due to particles from active regions, some probably originating from interplanetary acceleration processes. One of these events (January 1975) will be discussed in a subsequent paper by Richter et al. (1975). The others will be dealt with in forthcoming work.

The importance of having high time resolution, high angular resolution and the capability of determination of energy spectra from different directions, is obvious from the examples shown above. It is this tool, which will enable more distinct conclusions on details of interplanetary low energy particle propagation and behaviour.

This work has been supported in part by the Bundesminister für Forschung und Technologie through grants RS-12, WRS-10/7 and WRS-10/8.

References

Ipavich, F.M.: The Compton-Getting effect for low energy particles. Geophys. Res. Lett. **1**, 149–152, 1974

Keppler, E., Nielsen, E., Richter, K., Umlauft, G., Wilken, B., Williams, D.J.: Directional variations of proton energy spectra. Presented at the 14th International Cosmic Ray Conference, München, August 18–28, 1975

Keppler, E., Wilken, B., Richter, K., Umlauft, G., Fischer, K., Winterhoff, H.-P.: Ein Spektrometer für geladene Teilchen mittlerer Energie – Experiment E8 Helios –. Forschungsbericht des Bundesministers für Forschung und Technologie, BMFT-FB 76-14, 1976

Richter, K.: A method of calculating the pitch angle distribution of particle fluxes based on rocket and satellite data. IEEE Transact. Nucl. Science **NS-19**, Nr. 4, 32–36, 1972

Richter, A.K., Keppler, E., Richter, K., Wilken, B.: Observations of low-energy (>80 keV) protons ESP-shock spike-events in interplanetary space during January 6–8, 1975: Helios 1. J. Geophys., this issue, 1977

Sarris, E.T., Krimigis, S.M., Bostrom, C.O., Armstrong, T.P.: Simultaneous multispacecraft observations of energetic proton and electron bursts inside and outside the magnetosphere. J. Geophys. Res. to be published, 1977

Received January 31, 1977; Revised Version May 10, 1977